A finite element method for the geometric and material nonlinearities of concrete-filled steel tubular arches

Q. Wu
College of Civil Engineering, Fuzhou University, Fuzhou, China, E-mail: wuqingx@fzu.edu.cn

B. Chen
College of Civil Engineering, Fuzhou University, Fuzhou, China

K. Takahashi
Department of Civil Engineering, Faculty of Engineering, Nagasaki University, Nagasaki, Japan

ABSTRACT: A dual nonlinear finite element method based on fiber-model beam elements is presented for calculating the overall behaviour of a concrete-filled steel tubular (CFST) arch with precision. To account for geometric nonlinearity, an orientation matrix considering curvature in two moment directions and torsion angle is used to describe the changing status of incremental displacements and rotations, and a stiffness matrix including nonlinear terms for torsional and axial deformation is adopted. Introducing the general force and general strain of the section into the fiber-model beam elements yields the elasto-plastic tangent stiffness of the beam elements, which separates elastic and plastic deformation from the total deformation. This is proposed as a means of considering CFST material nonlinearity. The precision of the described method is verified through a case study in which the calculation results obtained using the CFST arch model agree well with the experimental values.

1 INTRODUCTION

A lot of concrete-filled steel tubular (CFST) arch bridges have been constructed in China since 1990. After a great deal of research, it has been found that material and geometric nonlinearities have a considerable effect on the load-carrying capacity of such bridges. Based on a lot of experimentation, the unified theories in which the CFST section is considered a single material or the theories in which stress-strain relation functions distinguish the steel and concrete have been developed (Zhong 1994, Cai 2003, Han 2004). Using the constitutive relations developed in this work, there are now two methods of applying finite element analysis to the material nonlinearity of a CFST arch: the plastic-hinge model and the fiber model.

The general plastic-hinge method uses the interaction between axial force and bending moment (N-M_y-M_z) to obtain the relationship between yield moment and approximate yield condition (Morris and Fenves 1970, Attalla et al. 1994, Hu et al. 2004). However, the establishment of yield surfaces is quite complicated and the stress or strain in the plastic-hinge model cannot be obtained directly. As compared with the plastic-hinge model, the fiber model requires numerical integration leading to time-consuming calculations. But in contrast to the fiber model, the stress-strain relation leads directly to evaluation of rigidity changes and the appearance of plastic deformation, so the combined action of axial force fluctuation and the biaxial moment is easily taken into account. Given this advantage, the fiber model is adopted here in seeking to account for the material nonlinearity of beam elements.

In the various fiber-model methods so far proposed (Zeng et al. 2003, Chen 2007, Yamato Engineering Inc. 2002) a geometric stiffness matrix considering the P-δ effect and a transformation matrix consisting of initial coordinate vectors are adopted to account for the geometric nonlinearity of a CFST arch. High-order nonlinear terms in the stiffness matrix and

the deformed coordinate vector in the transformation matrix should be considered in the buckling analysis of the arch structure (Pi and Bradford 2003).

In the references mentioned, material nonlinearity properties are taken into account by changing Young's modulus, E, in the elastic stiffness matrix, where E^e and E^p are the values of Young's modulus at the elastic stage and the plastic stage, respectively. This approach is easily convergent in the case of a simple stiffness matrix. But for a complex stiffness matrix (such as the stiffness matrix proposed by Maeda 1976), according to the authors' experience, iterative analysis converges with difficulty or barely at all.

In order to obtain more precise simulation of the nonlinearities of a CFST arch, a finite element method based on fiber-model beam elements is presented here that takes into account material and geometric nonlinearity. The corresponding FEM program *NL_Beam3D* is described and numerical analysis is carried out.

2 GEOMETRIC NONLINEARITY

The accuracy of geometric nonlinearity analysis relies on the accuracy of the stiffness matrix and the coordinate transformation matrix (Yang et al. 2003). This paper adopts Maeda's elastic stiffness matrix and Yoshida's coordinate transformation matrix. These matrices take the effects of high-order nonlinear terms and element transformations with arbitrary increments into consideration more accurately (Maeda and Hayashi 1976, Yoshida 1980).

2.1 Elastic stiffness matrix

The strain-displacement relationships at any point are:

$$\varepsilon_x = \frac{\partial u}{\partial x} + \frac{1}{2}\left(\frac{\partial v}{\partial x}\right)^2 + \frac{1}{2}\left(\frac{\partial w}{\partial x}\right)^2, \gamma_{xy} = \frac{\partial v}{\partial x} + \frac{\partial u}{\partial y}, \quad \gamma_{zx} = \frac{\partial u}{\partial z} + \frac{\partial w}{\partial x}, \quad \varepsilon_y = \varepsilon_z = \gamma_{yz} = 0 \tag{1}$$

where u, v, and w are displacements in the x, y, and z directions, respectively.

Using displacement components on neutral axes (u_0, v_0, w_0), angle components (θ_x, θ_y, θ_z), and a wrap function ω, the displacement functions are written as $u = u_0(x) + z\theta_y(x) - y\theta_z(x) + \theta_x'\omega(y,z)$, $v = v_0(x) - z\theta_x(x)$, $w = w_0(x) + y\theta_x(x)$. In accordance, the following equations are obtained:

$$\begin{aligned} \varepsilon_x &= u_0' - v_0'' y - w_0'' z + \frac{1}{2}\left(v_0'^2 + w_0'^2\right) + \underline{\frac{1}{2}\theta_x^2\left(z^2 + y^2\right) - \theta_x\left(v_0' z + w_0' y\right)} \\ \gamma_{xy} &= \theta_x'\left(-z + \frac{\partial \omega}{\partial y}\right), \quad \gamma_{zx} = \theta_x'\left(y + \frac{\partial \omega}{\partial z}\right) \end{aligned} \tag{2}$$

In these equations, $v_0' = \theta_z$ and $w_0' = -\theta_y$ are adopted. The underlined part of Eq. (2) is the torsional nonlinearity item neglected in some references.

Using the material law ($\sigma_x = E\varepsilon_x$, $\tau_{xy} = G\gamma_{xy}$, $\tau_{xz} = G\gamma_{zx}$) and the potential energy principle, the following equation is obtained:

$$\begin{aligned} U = {} & \frac{EA}{2}\int_0^l \left[(u_0')^2 + u_0'\left\{(v_0')^2 + (w_0')^2\right\} + \frac{1}{4}\left\{(v_0')^2 + (w_0')^2\right\}^2 \right] dx \\ & + \frac{EI_z}{2}\int_0^l \left[(v_0'')^2 + u_0'(\phi_0')^2 - 2v_0''w_0'\phi_0' + \underline{\frac{1}{2}\left\{(v_0')^2 + 3(w_0')^2\right\}(\phi_0')^2} \right] dx \\ & + \frac{EI_y}{2}\int_0^l \left[(w_0'')^2 + u_0'(\phi_0')^2 + 2v_0'w_0''\phi_0' + \underline{\frac{1}{2}\left\{3(v_0')^2 + (w_0')^2\right\}(\phi_0')^2} \right] dx + \frac{GJ}{2}\int_0^l (\phi_0')^2 dx + \underline{\frac{EI_r}{8}\int_0^l (\phi_0')^4 dx} \end{aligned} \tag{3}$$

Substituting the shape functions $u_0(x)=\alpha_1+x\alpha_2$, $v_0(x)=\alpha_3+x\alpha_4+x^2\alpha_5+x^3\alpha_6$, $w_0(x)=\alpha_7+x\alpha_8+x^2\alpha_9+x^3\alpha_{10}$, $\theta_x(x)=\alpha_{11}+x\alpha_{12}$ into Eq. (3) and using the minimum potential energy principle, the incremental equilibrium equation for a beam element is :

$$dQ = k_e \cdot dq^e = \left[k_0 + k_1(q^e) + k_2(q^e)\right] \cdot dq^e \tag{4}$$

where k_e is the incremental tangent stiffness matrix, dQ is the element force, q_e is the elastic displacement vector, k_0 is the linear term, and $k_1(q^e)$ and $k_2(q^e)$ are the first and quadratic nonlinear items of displacement q_e.

The equilibrium equation obtained from Eq. (4) is $Q=\left[k_0+1/2k_1(q^e)+1/3k_2(q^e)\right]\cdot q^e$.

2.2 Coordinate transformation matrix

The initial coordinate system of a beam element is shown in Fig. 1 (a). The initial coordinate vector is$\lambda_0=\{\lambda_{x0*}{}^T, \lambda_{y0*}{}^T, \lambda_{z0*}{}^T\}^T$. Also$\lambda_{x0*}$, λ_{y0*} and λ_{z0*} are 3×1 vectors, respectively, that can be derived by the Code Angle method.

The deformed coordinate vector is $\lambda=\{\lambda_{x*}{}^T, \lambda_{y*}{}^T, \lambda_{z*}{}^T\}^T$. As shown in Fig. 1 (b), the deformed element is defined by coordinate system (x_1', y_1', z_1') for node 1' and (x_2', y_2', z_2') for node 2'.

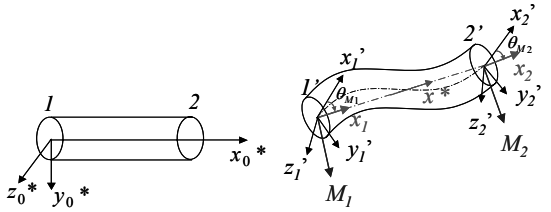

(a) Initial phase (b) Deformed phase

Fig.1 Local coordinate system

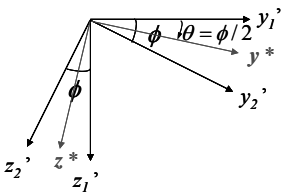

Fig.2 Torsional angle

The deformed coordinate vector λ is deduced as follows:

(1) Deformed vector x* is the unit vector linking node 1' with node 2'.

(2) For node 1', the rational angle θ_{M1} from axis x_1' to axis x_1 is calculated first. Then, the new coordinate system (x_1, y_1, z_1) is obtained by rotating coordinate system (x_1', y_1', z_1') with angle θ_{M1} around axis M_1. For node 2', the new (x_2, y_2, z_2) can be also obtained in a similar way.

(3) The plane formed by axis y_1' and axis z_1' of node 1' is parallel to the plane formed by axis y_2' axis and axis z_2' of node 2'. Therefore, the angle ϕ of axis y_1' to axis y_2' (or axis z_1' to axis z_2') can be obtained using vector analysis.

(4) In order to determine vector y* and vector z* in the deformed coordinates, it is assumed that the rotational angle θ_1* and θ_2* have the same absolute value but with reverse sign. As shown in Fig. 2, the deformed y* and z* are in the same direction as angle ϕ obtained in the above step.

Using this procedure, we find that the transformation matrix refers to the initial coordinate system. We can then consider variations in the two moment directions and torsional angle.

The rigid rotation vector ρ should be deduced after deformed coordinate vector λ is obtained. By rotating around axis L, vector (λ_{x0*}, λ_{y0*}, λ_{z0*}) in initial coordinate system moves to vector (λ_{x*}, λ_{y*}, λ_{z*}) in the deformed coordinate system. The rigid rotation vector is given by $\rho=\theta_L\lambda_L$, in which λ_L is the direction cosine of rotary axis L and θ_L is the rotation angle.

Finally, the deformation components at the two ends in the local coordinate system are:

$$\text{Displacements} \quad d_i{}^*{}_{(n)} = \{\lambda \cdot (x_i - x_1)\}_{(n)} - \{\lambda \cdot (x_i - x_1)\}_{(0)}$$

Rotations $$\theta_i *_{(n)} = \{\lambda \cdot (\theta_i - \rho)\}_{(n)} \quad (5)$$

where, i is the node number (i=1, 2), n is the number of equilibrium condition, 0 represents the initial condition.

It is found from Eq. (5) that the transformation matrix in the local coordinate system is not obtained using the initial transformation matrix in the global coordinate system, but using the relative difference between the deformed components and the initial components, such as (θ_i-ρ).

The transformation matrix proposed by Yoshida describes the deformed condition of a beam element using a coordinate system comprising three displacements and three rotational angles at the two ends of the element, not with three displacements only. Rigid rotation is separated from the deformed components. Furthermore, there is no accumulated error because the procedure is based on the initial coordinate system.

3 MATERIAL NONLINEARITY

In order to simply take into consideration material nonlinearity of a beam element, the elasto-plastic stiffness matrix is divided into separate elastic and plastic stiffness matrices, adopting the concepts of general force and general strain from beam element analysis. The total deformation can then be calculated as a sum of elastic and plastic deformation, while the internal force can be obtained from the product of the slope of elastic strain energy (elastic stiffness matrix) and deformation (Shugyo 2001). Using this method, the basic FEM formulation for CFST structures is presented on the basis of fiber-model beam elements.

3.1 Basic assumptions and fiber model

The basic assumptions are: (1) Plastic deformation components include the axial force, the moment around axis y^* and the moment around axis z^*; (2) No relative slip occurs between steel and concrete in the steel-concrete composite section.

The fiber model is based on the automatic integral of cross section. The cross section made up of fiber elements is divided into n sections. The stress and strain of every fiber is represented by the respective values of stress and strain at the center point of the fiber. Since the fiber model neglects the fibers' own rigidity, the division into fibers should be relative fine so as to satisfy the equivalent cross section properties.

3.2 Plasticity coefficient matrix of cross section

The general force f and general strain δ are defined according to Chen and Atsuta 1977. Based on assumption (1), the general force f and general strain δ are $f=\{f_x\ m_y\ m_z\}^T$ and $\delta=\{\varepsilon_0\ \phi_y\ \phi_y\}^T$, respectively. The axial force is $f_x = \int \sigma \cdot dA$, the bending moment around axis y^* is $m_y = \int \sigma \cdot z^* dA$, and the bending moment around axis z^* is $m_z = -\int \sigma \cdot y^* dA$. The axial strain is $\varepsilon_0 = \frac{1}{A}\int \varepsilon \cdot dA$, the bending strain around axis y^* is $\phi_y = \frac{1}{A}\int \frac{\partial \varepsilon}{\partial z} dA$, and the bending strain around axis z^* is $\phi_z = -\frac{1}{A}\int \frac{\partial \varepsilon}{\partial y} dA$. When the section comprises steel and concrete, the integration range for general force and strain should include both steel and concrete parts as a composite section.

Whether it is a single material section or a composite materials section, the strain $\varepsilon=\varepsilon_0+z^*\phi_y-y^*\phi_y$ should be satisfied. Based on the von-Mises criterion, the plastic flow principle, and the Ziegler hardening principle, the incremental equation $d\sigma = E_t d\varepsilon$ can be obtained. Integrating this, following equation is obtained:

$$df = \mathbf{s} \cdot d\delta \quad (6)$$

where E_t is the hardening coefficient of every fiber in the uniaxial stress-strain relationship, $df=\{df_x\ dm_y\ dm_z\}^T$, and $d\delta=\{d\varepsilon_0\ d\phi_y\ d\phi_y\}^T$. $\boldsymbol{s}$ has the dimension 3×3.

The total general strain $d\delta$ is the sum of the elastic general strain $d\delta^e$ and the plastic general strain $d\delta^p$ ($d\delta=d\delta^e+d\delta^p$), and $df=s_e \cdot d\delta^e$. Substituting those equations into Eq.(6), the following equation is obtained as:

$$d\delta^p = \mathbf{s}_p \cdot df = \left(\mathbf{s}^{-1} - \mathbf{s}_e^{-1}\right) \cdot df \tag{7}$$

where $\boldsymbol{s}_p$ is defined as the sectional plastic matrix, and $\boldsymbol{s}_e$ is the sectional elastic matrix.

3.3 Elasto-plastic tangent stiffness matrix of beam element

In order to separate the plastic stiffness matrix k_p (Young's modulus E^p) and the elastic stiffness matrix k_e (Young's modulus E^e) from the stiffness matrix of beam element, the plastic stiffness matrix k_p is obtained based on the sectional general force and strain, then the elasto-plastic tangent stiffness matrix $\boldsymbol{k}_{ep}$ is obtained.

Based on assumption (1), the incremental plastic deformations $dq_1{}^p$ at node 1 and $dq_2{}^p$ at node 2 in an element are:

$$dq_1{}^p = \left\{du^p{}_1 \quad 0 \quad 0 \quad 0 \quad d\theta^p{}_{y,1} \quad d\theta^p{}_{z,1}\right\}^T \text{ and } dq_2{}^p = \left\{du^p{}_2 \quad 0 \quad 0 \quad 0 \quad d\theta^p{}_{y,2} \quad d\theta^p{}_{z,2}\right\}^T \tag{8}$$

Because the dimension of $dq_1{}^p$ or $dq_2{}^p$ is 6, the corresponding sectional plastic matrix $\boldsymbol{k}_{p,1}$ or $\boldsymbol{k}_{p,2}$ changes from 3×3 (dimension of $\boldsymbol{s}_{p,1}$ or $\boldsymbol{s}_{p,2}$) to 6×6.

The relationship between general strain and displacement at the two ends of a beam element is:

$$dq^{p}{}_1 = \frac{l}{8}\left(3k_{p,1} \cdot dQ_1 - k_{p,2} \cdot dQ_2\right), \quad dq^{p}{}_2 = \frac{l}{8}\left(3k_{p,2} \cdot dQ_2 - k_{p,1} \cdot dQ_1\right) \tag{9}$$

where $dQ_1 = \left\{f_{x,1} \quad f_{y,1} \quad f_{z,1} \quad m_{x,1} \quad m_{y,1} \quad m_{z,1}\right\}^T$ and $dQ_2 = \left\{f_{x,2} \quad f_{y,2} \quad f_{z,2} \quad m_{x,2} \quad m_{y,2} \quad m_{z,2}\right\}^T$.

Therefore, the plastic deformation dq^p can be obtained as:

$$dq^p = k_p dQ \tag{10}$$

where $dq^p = \left\{dq^p{}_1 \quad dq^p{}_2\right\}^T$, $dQ = \left(dQ_1 \quad dQ_2\right)^T$ and $k_p = \frac{l}{8}\begin{bmatrix} 3k_{p,1} & -k_{p,2} \\ -k_{p,1} & 3k_{p,2} \end{bmatrix}$.

Given that the total incremental displacement dq is the sum of the incremental elastic displacement dq^e and the incremental plastic displacement dq^p ($dq=dq^e+dq^p$), and using Equation (4) ($dQ=k_e dq^e$), the following equation is obtained:

$$dQ = k_{ep} \cdot dq = \left(I + k_e k_p\right)^{-1} k_e \cdot dq \tag{11}$$

where $\boldsymbol{k}_{ep}=(I+k_e k_p)^{-1}k_e$ is defined as the elasto-plastic tangent stiffness matrix of a beam element, and includes the plastic stiffness matrix $\boldsymbol{k_p}$ and the elastic stiffness matrix $\boldsymbol{k_e}$. When the material is elastic, $\boldsymbol{k}_{ep}$ is the elastic tangent stiffness matrix $\boldsymbol{k}_e$. When the material becomes plastic, the plastic stiffness matrix $\boldsymbol{k}_p$ can be calculated directly using Eq. (10).

This makes it convenient to use this method to separate the plastic deformation and elastic deformation from the total deformation. The internal force can be obtained from the slope of elastic strain energy, and then the unbalanced forces during iterative analysis can be calculated accurately and quickly.

4 EXAMPLES AND DISCUSSIONS

Using the method described above, the 3D finite element program named *NL_Beam3D* (*N*on*L*inear analysis program of *Beam3D*) was developed to carry out analysis of CFST arches taking geometric and material nonlinearity into account. The materials laws adopted in the program are bi-linear and tri-linear models for steel (kinematic or isotropic hardening) with secondary parabola and exponential models for concrete (hardening criteria proposed by Ristic et al. 1986). Incremental-iterative nonlinear analysis makes use of the Newton load control method, the displacement control method, and the generalized displacement control method (Yang and Shieh 1990).

4.1 In-plane buckling of elastic arch

The first numerical example concerns a circular arch with a span of 160 inches (406.4 cm) and rise of 40 inches (101.6cm). The cross section is square, with b=h= 1 inch (2.54 cm). Young's modulus is 10^7 psi (6.896×10^6 N/cm^2). The load-displacement curves calculated by the *NL_Beam3D* program and the results given the perturbation method (Li and Shen 2000) are shown in Fig.3.

When a hinged arch is subjected to a central concentrated load in the vertical direction, the calculated load-deflection curve shows that the buckling type of the hinged arch is the bifurcation buckling. The buckling load obtained by the present model is close to the results in Li and Shen 2000.When this arch is fixed at both ends, the buckling becomes the limit-point buckling. The result obtained by the present model agrees well with that in Li and Shen 2000.

Therefore, the present model can be used to the analysis of in-plane bifurcation buckling and limit-point buckling.

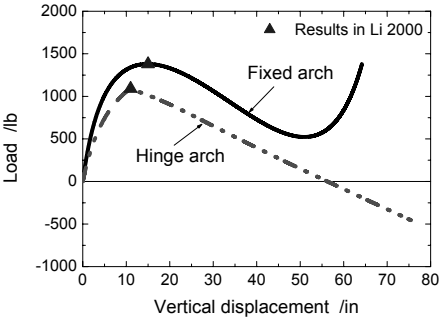

Fig.3 In-plane buckling of elastic arch

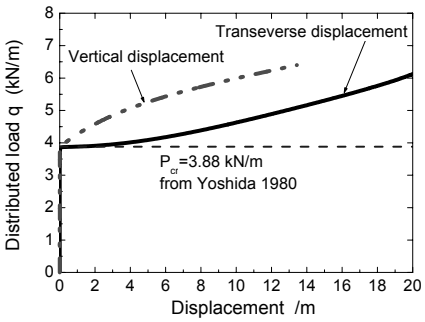

Fig.4 Out-of-plane buckling of elastic arch

4.2 Out-of-plane bifurcation buckling of elastic arch

Another numerical example concerns the out-of-plane bifurcation buckling of a fixed parabolic arch. The span is 100 m and the rise-to-span ratio is 0.3. The sectional axial rigidity is 0.4×10^7 kN. The in-plane and out-of-plane flexural rigidities are 0.1×10^7 kN-m^2 and 0.1×10^6 kN-m^2, respectively. The torsional rigidity is 0.1×10^6 kN-m^2. A uniformly distributed load is applied in the vertical direction. In order to initialize out-of-plane deflection of the arch, a uniformly distributed load with a magnitude 10^{-5} kN/m serving as an imperfection is applied in the out-of-plane direction.

The results for the load-deflection relationships obtained by present model are shown in Fig. 4. The bifurcation buckling load is determined from the load-deflection curve. The critical load is about 3.87kN/m, which is almost same as the value using the eigenvalue method obtained by Yoshida et al. 1980. So the present model can be used to the analysis of out-of-plane bifurcation buckling.

4.3 Experiment of CFST arch subjected to a concentrated load

An experiment using a CFST fixed parabolic arch subjected to a concentrated load was carried out at Fuzhou University in China (Chen 2007). The clear span is 4.600 m, and the rise is 1.533 m. The diameter of the steel tube is 76 mm and the thickness is 3.792 mm. Young's modulus of the steel tube is 206 GPa, and the yield stress is 307.67 MPa. The compressive strength of the concrete is 36.8 MPa. A concentrated load is applied at the arch crown or the one-quarter point. In the present analysis, the elastic perfect plastic model is used for the steel tube. The secondary parabola model is used for the infilled concrete.

The load- deflection curves obtained by the *NL_BEAM3D* and in the experiment are shown in Fig.5. It is obvious that the analysis is able to depict the test results to a very good degree of accuracy. Thanks to the general displacement control method used in the incremental-iterative nonlinear analysis, the post-buckling behavior of the arch could be automatically tracked and described.

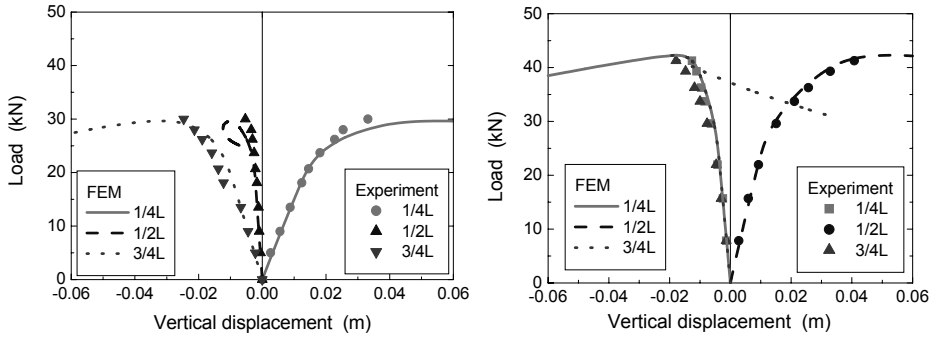

(a) Loading at one-quarter point (b) Loading at arch crown

Fig. 5 Load-deflection curves in CFST arch experiment

5 CONCLUSIONS

Using fiber-model beam elements that incorporate geometric and material nonlinearity, a basic formulation of the finite element method for CFST arches is presented. Geometric nonlinearity is taken into account by adopting an orientation matrix that considers curvature in two moment directions and torsional angle used to describe the changing status of incremental displacements and rotations. The stiffness matrix includes nonlinear items for torsional and axial deformation. Material nonlinearity is taken into account by incorporating the general force and general strain of a section into a fiber-model beam element, yielding the elasto-plastic tangent stiffness of the beam element that separates elastic and plastic deformation from the total deformation of the CFST.

A FEM program named *NL_BEAM3D* is developed based on these methods. By comparing the results obtained using this program with the results of experiments on CFST arches under concentrated loading, the precision of the program is verified.

REFERENCES

Attalla, M.R., Deierlein, G.G. and McGuire, W. 1994. Spread of plasticity: Quasi-plastic-hinge approach. *Journal of the Structural Division*, *ASCE* 120(8), p. 2451-2473.

Cai, S. 2003. *Modern concrete-filled steel tubular structure*. Beijing: People's traffic Press. (in Chinese)

Chen, B. 2007. *Concrete-filled steel tubular arch bridge (second edition)*. Beijing: People's traffic Press. (in Chinese)

Chen, W.F. and Atsuta, T. 1977. *Theory of beam-columns*, *Vol.2*: *Space behaviors and design*. McGraw-Hill International Book Company.

Han, L. 2004. *Concrete-filled steel tubular structure -theory and practice*. Beijing: Science Press. (in Chinese)

Hu, S., Su, H. and Wang J. 2004. 3D elastic-plastic seismic response analysis for CFST bridge. *China Highway Journal* 17(1), p. 57-61. (in Chinese)

Li, Y. and Shen, Z. 2000. Application of perturbation methods bifurcation instability problem. *Chinese Quarterly of Mechanics* 21(4), p. 497-5023. (in Chinese)

Maeda, Y. and Hayashi, M. 1976. Finite displacement analysis of space framed structures. *Journal of Structural Mechanics and Earthquake Engineering*, *JSCE* 253, p. 13-27. (in Japanese)

Morris, G.A. and Fenves, S.J. 1970. Elastic-plastic analysis of frameworks. *Journal of the Structural Division*, *ASCE* 96(ST5), p. 931~946.

Pi, Y.L. and Bradford, M.A. 2003. Elastic-plastic bucking and postbucking of arches subjected to a central load. Computer & Structures 81, p. 1811-1825.

Ristic, D., Yamada, Y. and Iemura H. 1986. Stress-strain based modeling of hysteretic structures under earthquake induced bending and varying axial loads. *School of Civil Engineering, Kyoto University*.

Shugyo, M. 2001. Elasto-plastic analysis of 3D steel frames with semi-rigid joint. *Report of Faculty of Engineering*, *Nagasaki University*, 31(57), p. 61-70.

Yamato Engineering Inc. 2002. *Manual of Y-Fiber3D Basic Version*.

Yang, Y.B. and Shieh, M.S. 1990. Solution method for nonlinear problems with multiple critical points. *AIAA Journal* 28(12), p. 2110-2116.

Yang, Y.B., Yau, J.D. and Leu, L.J. 2003. Recent developments in geometrically nonlinear and postbuckling analysis of framed structures. *Applied Mechanics Reviews* 56(4), p. 431-449.

Yoshida, Y., Masuda, N., Morimoto, T. and Hirosawa, N. 1980. An incremental formulation for computer analysis of space framed structures. *Journal of Structural Mechanics and Earthquake Engineering*, *JSCE* 300, p. 21-32. (in Japanese)

Zeng, G., Fan, L. and Zhang, G. 2003. CFST arch composite beam element analysis of the ultimate strength. *Railway Journal* 25(5), p. 97-102. (in Chinese)

Zhong, S. 1994. *Concrete-filled steel tubular structures*. Harbin: Heilongjiang Science and Technology Press. (in Chinese)